European Journal of Radiology 116 (2019) 27–33

Contents lists available at ScienceDirect

European Journal of Radiology

journal homepage: www.elsevier.com/locate/ejrad

Research article

Intra- and inter-observer variability in dependence of T1-time correction for common dynamic contrast enhanced MRI parameters in prostate cancer patients

Michaela Daniel[a,b], Stephan H. Polanec[a,c], Georg Wengert[a,c], Paola Clauser[c], Katja Pinker[c], Thomas H. Helbich[c], Dietmar Georg[a,b], Pascal A.T. Baltzer[a,c,*]

[a] Christian Doppler Laboratory for Medical Radiation Research for Radiation Oncology, Medical University of Vienna, Austria
[b] Department of Radiotherapy, Medical University of Vienna/AKH Vienna, Austria
[c] Department of Biomedical Imaging and Image-Guided Therapy, Medical University and General Hospital of Vienna, Austria

ARTICLE INFO

Keywords:
DCE
Quantitative imaging
T1-mapping
Multiple flip angle
Reproducibility

ABSTRACT

Background: Dynamic contrast enhanced (DCE) MRI parameters are potential biomarkers to characterise tumour vasculature and distinguish it from the non-cancerous blood vessel system within the prostate. However, the inevitable presence of intra- and inter-observer variabilities is challenging in this context. Additionally, pre-contrast T1-time correction is a prerequisite to gain quantitative DCE parameters in the first place. The current study investigated the effect of individualized T1-time correction on intra- and inter-reader variability for quantitative DCE-parameters in prostatic lesions.

Methods: In this IRB-approved retrospective study, two experienced radiologists assessed DCE parameters using individually measured (A) and fixed (B) T1-times twice with a time difference of three weeks. The dataset consisted of 35 MRI-guided biopsy-proven prostate cancer lesions. Limits of agreement (LoA) and coefficients of variability (CoV) were calculated to assess intra- and inter-reader variabilities of the parameters.

Results: With exception of k_{ep}, for all DCE parameters both intra- and inter-reader CoV were smaller in B compared to A. Absolute k_{ep} values were largely insensitive to T1-time correction induced bias. The mean intra-reader CoVs [5%, 95% percentile] (over all four DCE parameters and both readers) were 6.7% [0.5%, 15.1%] in A and 3.9% [0.2%, 11.0%] in B. The inter-reader CoVs were 9.0% [0.6%, 25.8%] (A) and 7.0% [0.3%, 25.4%] (B).

Conclusions: T1-time correction has a significant influence on the intra- and inter-reader variability. By applying individually measured T1-time correction, both intra- and inter-observer variability were found to increase. Out of all investigated DCE parameters, k_{ep} is the most robust to this investigated bias.

1. Introduction

In the field of functional imaging for oncologic purposes in the prostate, dynamic contrast enhanced (DCE) magnetic resonance imaging (MRI) has an important status. While there is ongoing debate about the necessity of DCE in prostate imaging for the task of cancer detection in PI-RADS v2 [1], its application in cancer staging, pharmacological and radiation therapy planning and monitoring is valued [2]. DCE MRI primarily differentiates the tumour vasculature from the non-cancerous blood vessel system within the prostate through measuring perfusion and vascular permeability [11]. Coherently, correlations between DCE MRI and histopathologic microvascularity parameters were found [12]. Higher microvessel density was found to be associated with the probability for metastases and higher Gleason scores. Additionally, the number of abnormal vessels observed in a tumour inversely correlates with the prognosis [13]. These coherences make DCE MRI parameters a potential powerful biomarker to predict and monitor therapy effects e.g. in radiation oncology.

Overall, there are three methods for analysing DCE MRI: qualitative, semi-quantitative, and quantitative. For qualitative analysis the contrast agent enhancement curve is visually inspected and assigned to a certain type. Many investigators have proposed semiquantitative measures, because these methods do not require assumptions about individual tissue anatomy and physiology [3,4]. Instead, the data are

* Corresponding author at: Department of Biomedical Imaging and Image-Guided Therapy, Medical University of Vienna, Währinger Gürtel 18-20, 1090, Wien, Austria.
E-mail address: pascal.baltzer@meduniwien.ac.at (P.A.T. Baltzer).

https://doi.org/10.1016/j.ejrad.2019.04.015
Received 28 December 2018; Received in revised form 13 April 2019; Accepted 22 April 2019

described through phenomenological parameters, which allow some interpretation towards tissue parameters. The most commonly used semiquantitative parameter is the initial area under the enhancement curve (iAUC) for the first 60 or 90 s. For quantitative analysis, pharmacokinetic models are applied to the imaging data. The most common model for this purpose is the Tofts model that assumes two compartments [5]. Volume transfer constant (k^{trans}), rate constant (k_{ep}) and extracellular plasma volume (v_e) are quantitative parameters that can be derived from the Tofts model. While the Prostate Imaging Reporting and Data System (PI-RADS) favours the qualitative method, a quantitative analysis should be preferred when aiming for establishment of DCE imaging biomarkers [1,6]. A prerequisite to gain quantitative parameters from dynamic image intensity in DCE MRI images is precontrast T1-time correction [7,8]. This is due to the fact that DCE image intensities do not reflect the contrast agent concentration proportionally in tissues and therefore cannot be used directly for kinetic model fitting. Among several T1 measurement methods, the multiple flip angles (MFA) [9,10] technique has been applied widely in current clinical practice for spoiled gradient echo sequences due to its higher signal-to-noise ratio and improved time efficiency.

Recently, initiatives like the Quantitative Imaging Biomarkers Alliance (QIBA) seek to identify sources of variation that may contribute to the overall measurement error [14,15]. These standardization initiatives are crucial to permit comparison of DCE MR imaging studies independent of imaging platforms, clinical sites, and time of imaging. Numerous sources of variation have been assessed with respect to their influence on pharmacokinetic parameter reproducibility [16–21]. It has been recognized that T1-time correction is a major contributing factor for the accuracy of kinetic parameter fitting in DCE MRI and the dominating source for kinetic parameter estimation errors [22]. Other sources of influence are patient motion, arterial input function (AIF) extraction, B1 field inhomogeneity or insufficient temporal resolution. Although contrast-enhanced MRI has been a workhorse in clinical MRI for quite some time, the use of the data was mostly of qualitative nature. A challenge for any quantitative approach to DCE image analysis is the inevitable presence of intra- and inter-observer variabilities. Quentin et al. found for a qualitative scoring assessment of enhancement curve in prostate cancer patients that the kappa value expressing inter-observer reliability was 0.77 for DCE MRI [23]. However, inter- as well as intra-observer variabilities of quantitative DCE parameters for prostate cancer have received little attention so far.

The aim of this study was to investigate the influence of T1-time correction on inter- and intra-observer variabilities of common quantitative dynamic contrast enhanced parameters in prostate cancer patients. Our hypothesis was that MFA T1-time correction introduces an additional factor of uncertainty that contributes to the overall variability and reduces reproducibility.

2. Material and methods

2.1. Patients

In this IRB-approved, retrospective study, 35 consecutive prostate cancer patients (mean age, 67 ± 13y, mean PSA 8.9 ± 4.4 ng/ml, histopathologically classified as Gleason score 3 + 3 in 12, Gleason score 3 + 4 in 7, Gleason score 4 + 3 in 7, Gleason score 4 + 4 in 3, Gleason score 4 + 5 in 5 and Gleason score 5 + 4 in 1 case; all stage T2) diagnosed during a 24-month time-period were investigated. The requirement for informed consent was waived by the IRB. All patients were diagnosed by MRI-guided, in-bore 18 G core biopsy [24]. Per lesion, at least three representative biopsy cores were obtained. The collected specimens were reviewed by a specialized urogenital pathologist using the criteria defined by the International Society of Urological Pathology-modified Gleason score classification [25].

2.2. MR imaging

All examinations were performed on a 3 T MRI system (MAGNETOM Trio Tim, Siemens Healthineers, Germany) in feet-first supine position. The vendor-supplied spine-array and flexible surface coils were used for image acquisition in a combined manner. No endorectal coil was used for the examinations. An antiperistaltic agent, 20 mg of Butylscopolaminiumbromid (Buscopan®, Boehringer Ingelheim, Germany), was injected intramuscular and patients had to empty their bladder before the scan. The rectum was filled with ultrasound gel to improve the image quality and avoid air bubbles. T1-time correction sequences were applied before dynamic scanning using the variable flip-angle method (TR/TE 3.85/1.42; four flip angles at 2°, 5°, 10° and 20°; matrix 256; FOV 260 mm; slice thickness 3.6 mm; acquisition time 2:47 min). A three-dimensional, view-sharing, T1-weighted gradient echo sequence (TWIST) was used for DCE scanning. In order to achieve high spatial and temporal resolution, the first acquisition of a high resolution k-space mask was followed by repetitive subsampled central k-space acquisitions (TR/TE 3.85/1.42; flip angle 12°; GRAPPA factor 2; 70 repetitions; TWIST k-space subsampling with central region A 30% and sampling density 25%, resulting in a temporal resolution of 4.22 s; FOV 260 mm; matrix 160, overall time of acquisition: 5 min). Gadoterate meglumine (Gd-DOTA, Dotarem®, Guerbet, France) was injected after three baseline scans intravenously as a bolus (0.2 ml/kg body weight) using a power injector (Spectris, Medrad, Pittsburgh, PA) at a flow rate of 4 ml/s, followed by a flush of 20 ml of saline solution.

2.3. Pharmacokinetic model and T1-times correction

Volume transfer constant (k^{trans}), rate constant (k_{ep}), fractional volume of extravascular extracellular space (v_e) and initial area under the enhancement curve (iAUC) were calculated with the Tissue 4D software tool (Syngo, Siemens Healthineers, Germany) based on the standard Tofts model [5]. The arterial input function (AIF) was derived manually from the femoral artery. Two sets of T1-time corrected datasets were calculated: First, an individualized T1-time correction was performed in line using the variable flip angle method (in the further manuscript these data are referred to as $T1_{individualized}$). This method relies on the acquisition of proton density and T1-weighted images at several flip angles. From the resulting images, a voxelwise T1 map is calculated based on a regression analysis of the flip angle dependent signal alteration. Besides the acquisition of the variable flip angle data, the used software can calculate the resulting T1 map in less than a minute, most of this being operating time; no extra processing time is otherwise required. Second, DCE data underwent the same pharmacokinetic modelling process using a predefined population based fixed T1-time of 1500 ms (in the further manuscript these data are referred to as $T1_{fixed}$). Both approaches are employed within the vendor-supplied Tissue 4D toolbox.

2.4. Image analysis

Lesions were independently assessed by two radiologists (reader 1 = R1; reader 2 = R2; with 5 years of experience in abdominal MRI, each) on a dedicated workstation (Syngo, Siemens Healthineers, Germany) for both individually T1-time corrected ($T1_{individualized}$) data and fixed T1-time corrected ($T1_{fixed}$) data.

Lesions were identified on early contrast-enhanced images (90 s. after contrast medium application) considering the information from the subsequent in-bore MRI-guided biopsy examination where the biopsied lesion was documented. The readers drew a circular region of interest (ROI) around the respective lesion on the early enhanced images and copied the ROI to the calculated two datasets of parametric maps ($T1_{individualized}$ and $T1_{fixed}$). In case of unspecific enhancement, the readers could also consider T2-weighted and DWI/ADC information to localize the lesion. Lesions that could not be identified in an

unequivocal manner were excluded. k^{trans}, k_{ep}, v_e and iAUC were assessed in the two-dimensional ROI. The ROI avoided non-enhancing lesion parts and ranged in size between 10 and 80 mm^2 (corresponding to approximately 3–10 mm axial lesion diameter). The ROIs were chosen as large as possible but did not exceed 10 mm in axial diameter due to the circular configuration and the need to exclude non-enhancing tissue. Both readers repeated the measurements after three weeks. A third radiologist with more than 10 years of experience in urogenital imaging supervised the reading process and checked the ROI positions for consistency with the biopsied lesion. This reader did only check the ROI positions and did not intervene with the reading process.

2.5. Statistical analysis

SPSS 19.0 (IBM Corp., Armonk, NY, USA) was used for statistical analysis. The statistical calculations were performed on a per-lesion basis (one primary lesion per patient). Bland Altman plots were generated and upper and lower limits of agreement (LoA) as percentage of the patient mean value were extracted. The coefficient of variability (CoV) was calculated as the ratio of the standard deviation to the mean (CoV = SD/mean). The LoA and the CoV were calculated as measures for inter- and intra-observer agreement and summarized in a Forest plot. Spearman correlation coefficients were calculated to determine the correlation of $T1_{fixed}$ and $T1_{individualized}$ parameters for each reader using the mean value of the two measurements. The significance threshold for all tests was $p < 0.05$.

3. Results

All lesions showed positive enhancement on baseline DCE images and could be clearly localized. There were no major discrepancies between lesion localizations of the ROIs of both readers.

3.1. Measured DCE parameters

All measurement results (means over the patient cohort) are presented in Table 1. Fig. 1 shows the evaluated parametric maps of one patient for $T1_{individualized}$ correction and $T1_{fixed}$ correction. The underlying clinical case is displayed in Fig. 2.

3.2. Correlation of $T1_{individualized}$ and $T1_{fixed}$ data

Fig. 3 illustrates the correlations of $T1_{individualized}$ and $T1_{fixed}$ data of all DCE parameters with scatter plots. The slope of linear fits for k^{trans}, v_e and iAUC is 2.8, 2.5 and 2.7, respectively, while for k_{ep} the linear fit slope equals 1 (see Fig. 3). The mean Spearman correlation coefficients of $T1_{individualized}$ and $T1_{fixed}$ data are 0.57 for k^{trans}, 0.99 for k_{ep}, 0.64 for v_e and 0.59 for iAUC.

3.3. Intra- and inter-reader variability (LoA and CoV)

The forest plot of intra- and inter-reader reproducibility in terms of Bland Altman LoA for $T1_{individualized}$ and $T1_{fixed}$ parametric data is illustrated in Fig. 4. The corresponding exemplary Bland Altman plots of all parameters can be found in the Supplementary material (Fig. S1). The mean lower and upper intra-reader LoA (see Fig. 4, blue and red) over all four DCE parameters and both readers are $-27 \pm 6\%$–$33 \pm 9\%$ with a mean difference of $3 \pm 5\%$ for the $T1_{individualized}$ data and $-29 \pm 11\%$–$27 \pm 10\%$ with an overall mean difference of $-1 \pm 3\%$ for the $T1_{fixed}$ data. The equivalent measures for inter-reader variabilities (see Fig. 4, violet) are $-51 \pm 2\%$ to $43 \pm 6\%$ with a mean difference of $-4 \pm 3\%$ for the $T1_{individualized}$ and $-43\% \pm 11\%$ to $33 \pm 9\%$ data with a mean difference of $-5 \pm 2\%$ for the $T1_{fixed}$ data. When comparing the performance of the two readers, the intra-reader variability for reader 1 was insignificantly larger in the $T1_{fixed}$ data than in the $T1_{individualized}$ data (lower LoA: $-35 \pm 11\%$ vs. $-29 \pm 5\%$), while it was significantly smaller ($p = 0.045$) for reader 2 over all DCE parameters (upper LoA: $20 \pm 6\%$ vs. $35 \pm 5\%$). Table 2 gives an overview of the resulting inter- and intra-reader variabilities for the mean and the 5% and 95% percentiles of the coefficients of variation (CoV) for all DCE parameters. Inter-reader variability is approximately 40% larger than intra-reader variability. With exception of k_{ep}, for all DCE parameters both intra- and inter-reader CoV are smaller in the not individually corrected

Table 1
Mean ± standard deviation of measured values for all four investigated parameters of first and second measurement (M 1, M 2) for both readers and fixed and individually corrected T1 data. In cases of statistically significant differences the significance levels by means of Wilcoxon Rank Sum tests are given, grey numbers indicate non-significant differences.

		$T1_{individualized}$			$T1_{fixed}$		
		reader 1	reader 2	inter sign	reader 1	reader 2	inter sign
k^{trans}	M 1	0.062±0.031	0.069±0.035	**p=0.041**	0.22±0.09	0.24±0.09	
	M 2	*0.061±0.031*	0.065±0.034		*0.22±0.09*	*0.25±0.09*	
	intra sign		**p=0.014**				
k_{ep}	M 1	0.55±0.27	0.57±0.27		0.60±0.26	0.61±0.30	
	M 2	*0.57±0.30*	0.59±0.29		*0.60±0.29*	0.64±0.29	
	intra sign		**p=0.049**			**p=0.003**	
v_e	M 1	0.16±0.07	0.16±0.08		0.47±0.13	0.50±0.14	
	M 2	*0.15±0.07*	0.15±0.07		*0.47±0.13*	0.48±0.13	
	intra sign		**p<0.001**			**p=0.015**	
iAUC	M 1	7.6±3.8	8.3±4.0		24.5±9.3	26.7±9.7	
	M 2	*7.4±3.7*	7.7±4.0		*24.6±9.1*	*27.2±9.9*	
	intra sign		**p=0.010**				

Intra sign = level of significance for intra-reader comparison, inter sign = level of significance for inter-reader comparison, k^{trans} = transfer constant, k_{ep} = rate constant, v_e = extracellular plasma volume, iAUC = initial area under the curve.

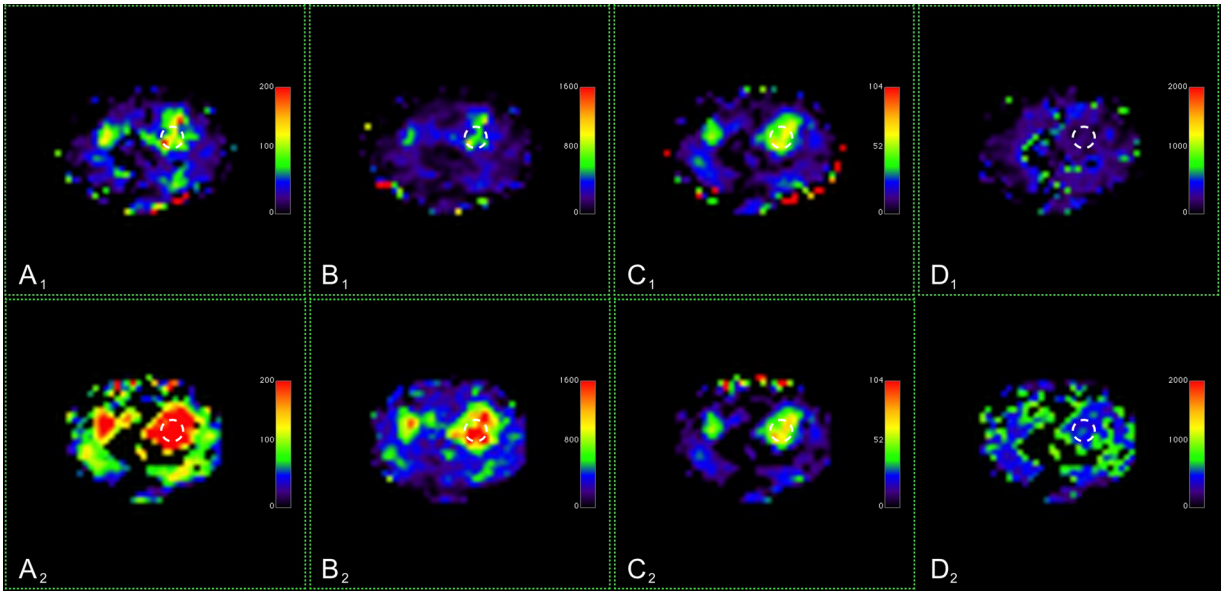

Fig. 1. In-bore biopsy proven Gleason score 4 + 4 (prognostic group 4) prostate cancer in the transitional zone of a 72-year old patient, PSA 16.2 ng/ml. Parametric maps of individualized T1 corrected (upper row, 1) and fixed T1 corrected data (lower row, 2). A represents k^{trans}, B iAUC, C k_{ep} and D v_e. As evidenced by the standardized window-center settings and given in the results section, the $T1_{fixed}$ dataset yielded systematically higher parameter values that cancelled themselves out in k_{ep} calculation with k_{ep} being k^{trans}/v_e. The Region of Interest (ROI) is indicated by a dashed circle and was copied without manual input directly from raw early enhanced DCE images to the parametric maps calculated from the raw DCE data.

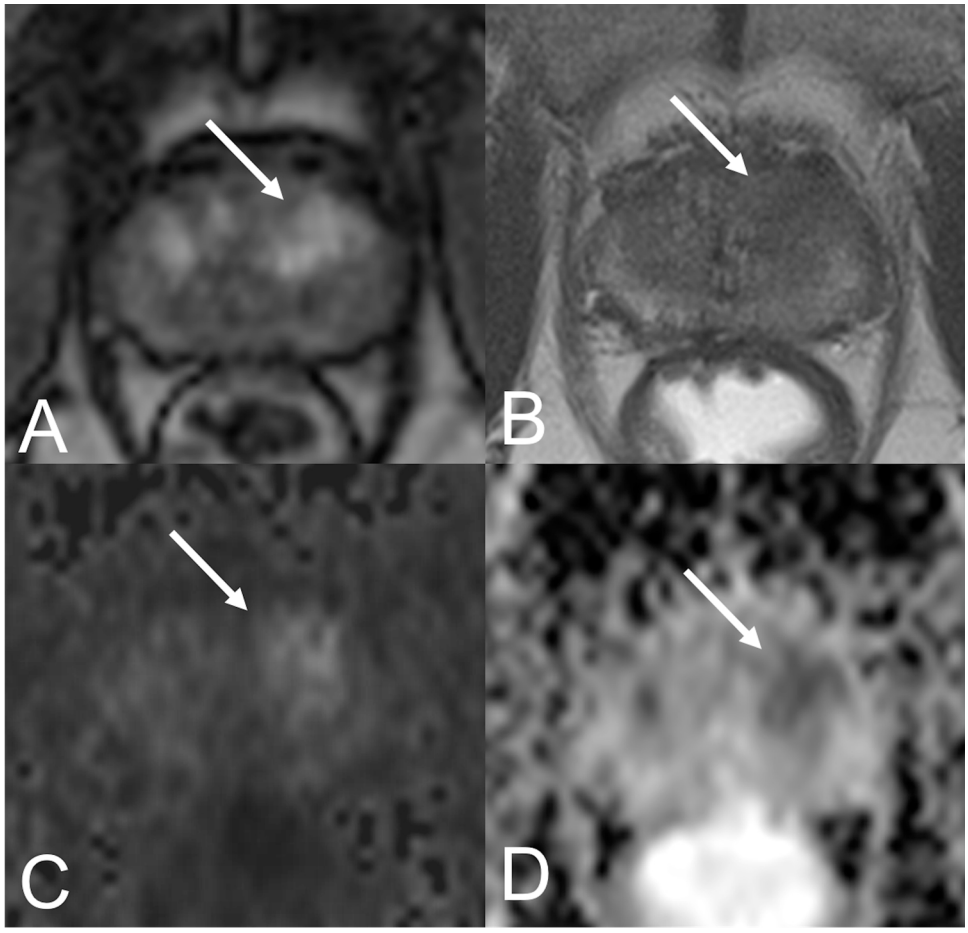

Fig. 2. 72-year old patient, PSA 16.2 ng/ml (same patient as in Fig. 3). After the examination, in-bore biopsy proved a Gleason score 4 + 4 (prognostic group 4) prostate cancer in the left transitional zone. The preinterventional MRI scan demonstrates early enhancement on DCE images (A), a non-circumscribed mass > 15 mm in size on T2w (B, PI-RADS 5), DWI hyperintensity (calculated b1400s/mm^2) and hypointensity on the ADC map (D), corresponding to DWI and overall PI-RADS 5.

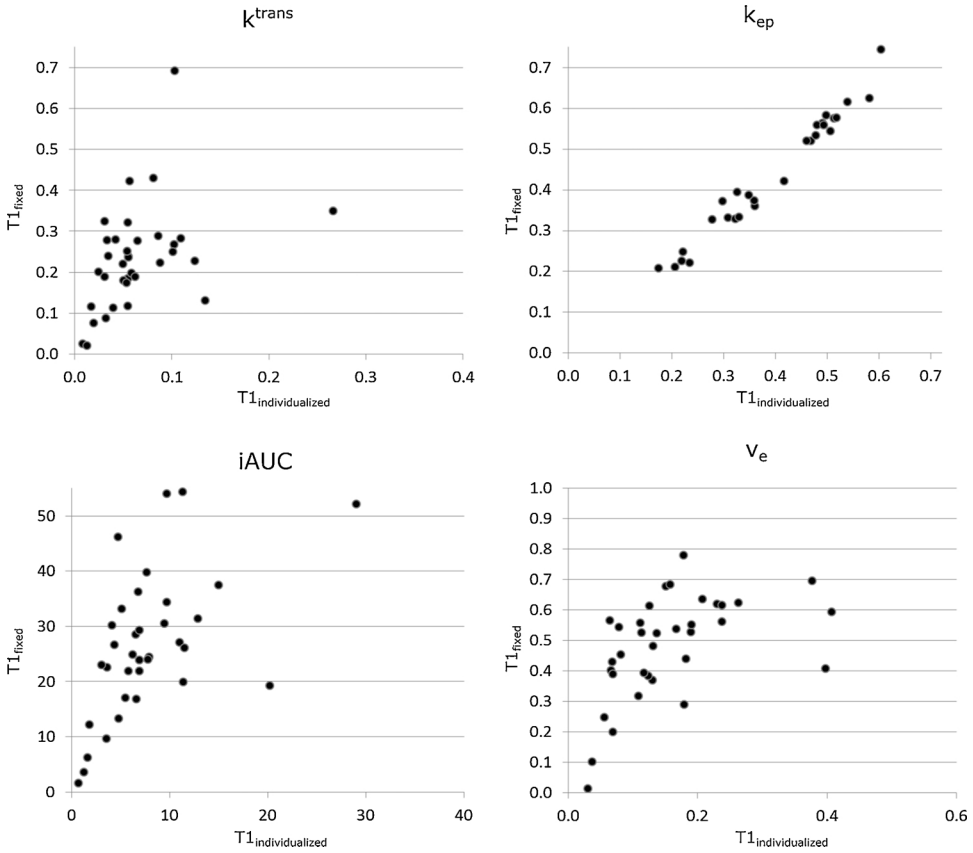

Fig. 3. Scatter plots to visualize the correlations of the investigated DCE parameters of the individualized T1 corrected data (y-axes) with the fixed T1 corrected data (x-axes). Each dot represents the mean of all four measurements (two measurements per reader). k^{trans} = transfer constant, k_{ep} = rate constant, v_e = extracellular plasma volume, iAUC = initial area under the curve.

dataset ($T1_{fixed}$).

4. Discussion

The importance of the reproducibility of imaging biomarkers is beyond debate, as any biomarker fails its purpose, if it is not reproducible and transferrable to other patients, scanners of different vendors and imaging protocols. In this context, there are many challenges regarding MRI biomarkers. Magnetic field and motion artefacts, different echo times, repetition times and other acquisition parameters, differences in technical equipment and also the use of different correction methods have impact on the resulting quantitative parameters. The sources of influence regarding DCE parameters additionally range from the AIF extraction over B1 field inhomogeneity up to insufficient temporal resolution. Mendichovszky et al. investigated the AIF reproducibility in the kidney-region of volunteers and found no significant difference between two operators [20]. Ashton et al. studied the inter-operator reproducibility of DCE parameters in tumours of the lung, liver and head and neck region and found that the median variability due to tumour margin identification was approximately 6% while the variability due to AIF identification was significantly lower [17]. Based on these two studies we can assume that the AIF extraction only plays a minor role in the intra- and inter-observer variability for the prostate cancer patients of the present study in comparison to the effect of the ROI delineation.

For primary prostate cancer detection, the value of DCE is considered rather small [1] or may even be considered negligible as some studies have shown that biparametric non-contrast approaches are not inferior to protocols including DCE in this setting [30]. Especially for radiotherapy purposes, DCE images are increasingly recognized as a potential tool for lesion contouring based on functional imaging findings. Rischke et al. compared DCE, DWI and T2-weighted contours of six observers for dominant intraprostatic lesion contouring and found that using the DCE images resulted in a higher agreement than using the T2-weighted images [27]. We are convinced that DCE MRI may be useful for upcoming dose-painting or dose escalation approaches of the dominant intra-prostatic lesion in radiotherapy of prostate cancer [28,29]. Current applications of DCE are summarized in [2].

This study investigated the influence of MFA-based T1-time correction on the reproducibility of DCE parameters in terms of inter- and intra-reader variability. Results showed superior reproducibility for the $T1_{fixed}$ data both in terms of inter- and intra-reader variability. These results indicate that the current clinical practice in which MFA corrections are applied with the aim to gain quantitative and comparable imaging parameters might have to be reconsidered. We confirmed our hypothesis that the T1-time correction introduces an additional factor of uncertainty that contributes to the reduction of overall reproducibility. This is due to the fact that both T1-time estimation using the signal acquired at variable flip angles and pharmacokinetic modelling of DCE curves require a regression analysis. Resulting parameters are fitted by least squares algorithms and each harbour a fitting error. This error sums up if both analyses are combined. The negative influence on inter- and intra-observer variability is reflected in higher coefficients of variation in all $T1_{individualized}$ DCE parameters and for both readers. Noticeable differences were found for the two readers in terms of how T1-time correction influenced their variabilities.

Davenport et al. determined the reproducibility of 'Time-Resolved Angiography with Interleaved Stochastic Trajectories' (TWIST)-derived quantitative DCE MRI in a uterine fibroid model and found that v_e was the most reproducible parameter [26]. In contrast, our results suggest that the reproducibility of the parameter is depending on the use of T1-time correction. In more detail, k_{ep} was found to be the most reproducible parameter for individually corrected data and v_e or k^{trans} for $T1_{fixed}$ data in terms of inter- or intra-reader reproducibility, respectively. Additionally, $T1_{individualized}$ and $T1_{fixed}$ data showed the highest correlation for the parameter k_{ep} (0.99), demonstrating its robustness to

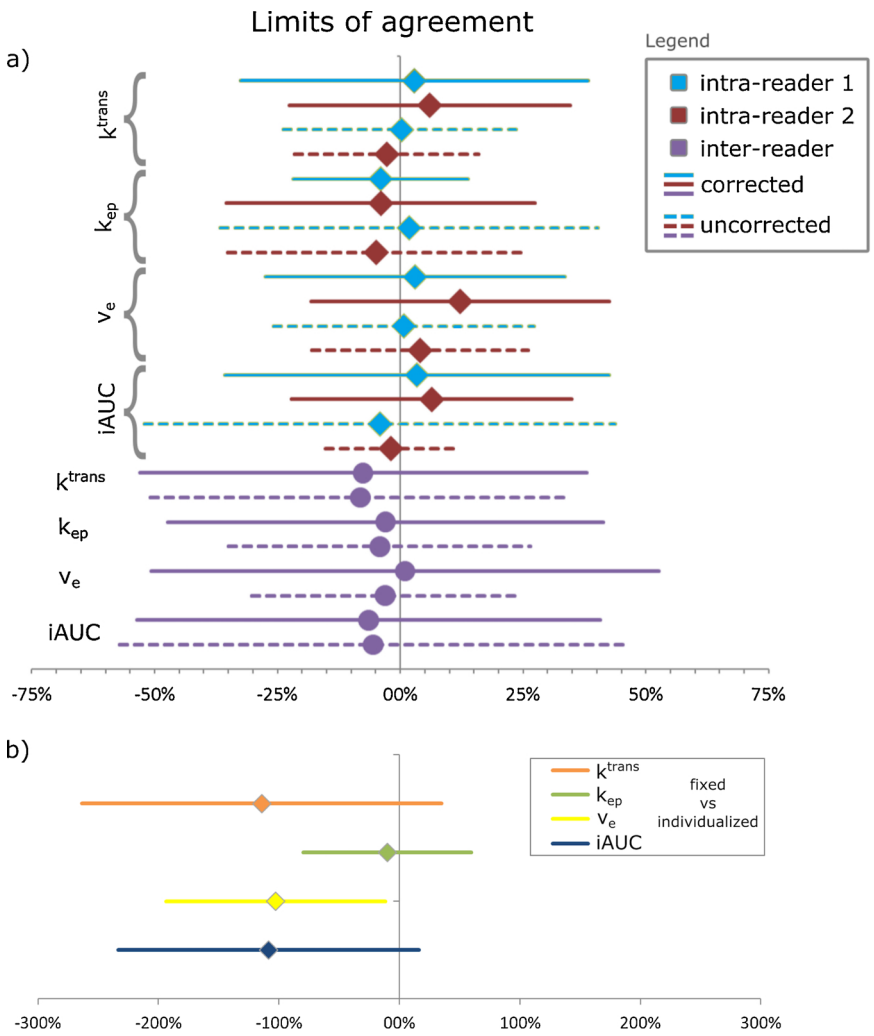

Fig. 4. Forest plot of Bland Altman limits of agreement of a) intra- and inter-reader reproducibility for individualized and fixed T1 corrected imaging data and b) in between fixed and individualized T1 corrected data. Abbreviations: k^{trans} = transfer constant, k_{ep} = rate constant, v_e = extracellular plasma volume, iAUC = initial area under the curve.

Table 2
Coefficients of variation (CoV) for the four investigated DCE parameters. The CoV means and 95% and 5% percentiles of intra- and inter-reader variabilities are presented. Mean CoV variabilities over all parameters are given in the last two lines.

Coefficients of variation (CoV)		$T1_{individualized}$			$T1_{fixed}$		
		mean	95%ile	5%ile	mean	95%ile	5%ile
k^{trans}	intra reader 1	**5.8%**	15.6%	0.0%	**3.3%**	7.7%	0.3%
	intra reader 2	**6.6%**	15.0%	0.6%	**2.5%**	6.7%	0.0%
	inter-reader	**8.2%**	22.4%	0.3%	**7.8%**	27.1%	0.3%
k_{ep}	intra reader 1	**3.7%**	9.7%	0.3%	**5.2%**	12.7%	0.2%
	intra reader 2	**4.2%**	8.5%	0.7%	**6.2%**	15.0%	0.0%
	inter-reader	**6.6%**	16.8%	0.1%	**6.3%**	24.6%	0.4%
v_e	intra reader 1	**7.3%**	13.9%	0.9%	**4.0%**	12.5%	0.2%
	intra reader 2	**9.5%**	20.6%	0.0%	**3.7%**	12.6%	0.0%
	inter-reader	**10.9%**	30.9%	0.9%	**5.6%**	21.2%	0.2%
iAUC	intra reader 1	**8.6%**	17.9%	0.1%	**4.4%**	15.0%	0.6%
	intra reader 2	**7.7%**	19.5%	1.4%	**2.2%**	5.6%	0.4%
	inter-reader	**10.1%**	33.1%	1.0%	**8.3%**	28.5%	0.4%
mean intra-reader variability		**6.7%**	15.1%	0.5%	**3.9%**	11.0%	0.2%
mean inter-reader variability		**9.0%**	25.8%	0.6%	**7.0%**	25.4%	0.3%

the T1-time correction. In comparison, the other DCE parameters showed Spearman correlation values of approximately 0.6. The difference between the variables was not random: k_{trans} and v_e values were significantly higher based on $T1_{individualized}$ calculation. The systematic difference between both T1-time correction methods is corroborated by comparable k_{ep} values. k_{ep}´s mathematical definition is $k_{ep} = k^{trans}/v_e$. Consequently, the variation introduced by T1-time correction cancel out. This could indicate that k_{ep} should get a more important role in future DCE evaluations.

Regarding the association between DCE parameters with each other, we found a strong positive correlation between k^{trans} and iAUC (˜0.9) that also has been recognized in previous studies [6,16]. Further, a weak negative correlation between v_e and k_{ep} (˜-0.5) and a weak positive correlation between v_e and iAUC (˜0.5) were found. These correlations are evident as $k_{ep} = k^{trans}/v_e$ and k^{trans} is strongly correlated to iAUC, as stated above.

The present study has some limitations. First, the study design was retrospective and the patient number is limited. The protocol in use for MFA-based T1-time correction was tailored to clinical needs and a more sophisticated approach using more flip angles might have yielded different and probably more accurate results. The fixed T1-time was not varied, thus no conclusions regarding optimal fixed T1-times for the $T1_{fixed}$ approach can be drawn. Second, delineations of primary lesions are dependent on data quality and observer experience. In our study,

the tumour location was determined by MRI-guided in-bore biopsy and both readers had comparable experience in the analysis of prostate MRI examinations. Thirdly, the prostate is prone to movement due to changes in rectal filling. We addressed this influence by application of an antiperistaltic agent and insertion of rectal gel.

5. Conclusions

The use of individualized T1-time correction has a relevant influence on the reproducibility of quantitative DCE MRI parameters. By applying individualized T1-time correction, both intra- and inter-observer variability were found to increase. Out of all DCE parameters, k_{ep} is the most robust to T1-time correction induced bias.

Conflicts of interest

The authors declare that there is no conflicts of interest.

Acknowledgement

The financial support by the Austrian Federal Ministry of Science, Research and Economy and the National Foundation for Research, Technology and Development is gratefully acknowledged.

Appendix A. Supplementary data

Supplementary material related to this article can be found, in the online version, at doi:https://doi.org/10.1016/j.ejrad.2019.04.015.

References

[1] J.C. Weinreb, J.O. Barentsz, P.L. Choyke, F. Cornud, M.A. Haider, K.J. Macura, D. Margolis, M.D. Schnall, F. Shtern, C.M. Tempany, H.C. Thoeny, S. Verma, PI-RADS prostate imaging - reporting and data system: 2015, version 2, Eur. Urol. 69 (2016) 16–40, https://doi.org/10.1016/j.eururo.2015.08.052.

[2] Y. Mazaheri, O. Akin, H. Hricak, Dynamic contrast-enhanced magnetic resonance imaging of prostate cancer: a review of current methods and applications, World J. Radiol. 9 (2017) 416–425, https://doi.org/10.4329/wjr.v9.i12.416.

[3] J.L. Evelhoch, Key factors in the acquisition of contrast kinetic data for oncology, J. Magn. Reson. Imaging 10 (1999) 254–259, https://doi.org/10.1002/(SICI)1522-2586(199909)10:3<254::AID-JMRI5>3.0.CO;2-9.

[4] M. Medved, G. Karczmar, C. Yang, J. Dignam, T.F. Gajewski, H. Kindler, E. Vokes, P. MacEneany, M.T. Mitchell, W.M. Stadler, Semiquantitative analysis of dynamic contrast enhanced MRI in cancer patients: variability and changes in tumor tissue over time, J. Magn. Reson. Imaging 20 (2004) 122–128, https://doi.org/10.1002/jmri.20061.

[5] P.S. Tofts, T1-weighted DCE imaging concepts: modelling, acquisition and analysis, MAGNETOM Flash 3 (2010) 31–39.

[6] N. Tau, A. Berlin, I. Yeung, J. Halankar, G. Murphy, S. Ghai, U. Metser, P.M. Hospital, M.S. Hospital, P. Margaret, C. Centre, Quantitative assessment of dynamic 18F-fluoromethycholine PET and dynamic contrast enhanced MRI in high risk prostate cancer, Br. J. Radiol. (2018) 20180568.

[7] P.S. Tofts, E.P.G.H. du Boulay, Towards quantitative measurements of relaxation times and other parameters in the brain, Neuroradiology 32 (1990) 407–415, https://doi.org/10.1007/BF00588474.

[8] N.G. Dowell, P.S. Tofts, Fast, accurate, and precise mapping of the RF field in vivo using the 180° signal null, Magn. Reson. Med. 58 (2007) 622–630, https://doi.org/10.1002/mrm.21368.

[9] D. Wang, L. Shi, Y.X.J. Wang, J. Yuan, D.K.W. Yeung, A.D. King, A.T. Ahuja, P.A. Heng, Concatenated and parallel optimization for the estimation of T1 map in FLASH MRI with multiple flip angles, Magn. Reson. Med. 63 (2010) 1431–1436, https://doi.org/10.1002/mrm.22294.

[10] G. Andreisek, L.M. White, Y. Yang, E. Robinson, H.-L.M. Cheng, M.S. Sussman, Delayed gadolinium-enhanced MR imaging of articular cartilage: three-dimensional T1 mapping with variable flip angles and B 1 correction, Radiology 252 (2009) 865–873, https://doi.org/10.1148/radiol.2531081115.

[11] D. Bonekamp, K.J. Macura, Dynamic contrast-enhanced magnetic resonance imaging in the evaluation of the prostate, Top. Magn. Reson. Imaging 19 (2008) 273–284, https://doi.org/10.1097/RMR.0b013e3181aacdc2.

[12] C.G. van Niekerk, J.A.W.M. van der Laak, T. Hambrock, H.J. Huisman, J.A. Witjes, J.O. Barentsz, C.A.H. Van de Kaa, Correlation between dynamic contrast-enhanced MRI and quantitative histopathologic microvascular parameters in organ-confined prostate cancer, Eur. Radiol. 24 (2014) 2597–2605, https://doi.org/10.1007/s00330-014-3301-z.

[13] A. Erbersdobler, H. Isbarn, K. Dix, I. Steiner, T. Schlomm, M. Mirlacher, G. Sauter, A. Haese, Prognostic value of microvessel density in prostate cancer: a tissue microarray study, World J. Urol. 28 (2010) 687–692, https://doi.org/10.1007/s00345-009-0471-4.

[14] D.C. Sullivan, N.A. Obuchowski, L.G. Kessler, D.L. Raunig, C. Gatsonis, E.P. Huang, M. Kondratovich, L.M. McShane, A.P. Reeves, D.P. Barboriak, A.R. Guimaraes, R.L. Wahl, Metrology standards for quantitative imaging biomarkers, Radiology 277 (2015) 813–825, https://doi.org/10.1148/radiol.2015142202.

[15] J.P.B.O. Connor, E.O. Aboagye, J.E. Adams, H.J.W.L. Aerts, S.F. Barrington, A.J. Beer, R. Boellaard, S.E. Bohndiek, M. Brady, G. Brown, D.L. Buckley, T.L. Chenevert, L.P. Clarke, S. Collette, G.J. Cook, M. Nandita, J.C. Dickson, C. Dive, J.L. Evelhoch, C. Faivre-finn, F.A. Gallagher, F.J. Gilbert, R.J. Gillies, V. Goh, J.R. Griffiths, A.M. Groves, S. Halligan, A.L. Harris, D.J. Hawkes, O.S. Hoekstra, E.P. Huang, B.F. Hutton, E.F. Jackson, G.C. Jayson, A. Jones, D. Koh, D. Lacombe, P. Lambin, N. Lassau, M.O. Leach, T. Lee, E.L. Leen, J.S. Lewis, Y. Liu, M.F. Lythgoe, P. Manoharan, R.J. Maxwell, K.A. Miles, B. Morgan, S. Morris, T. Ng, A.R. Padhani, G.J.M. Parker, M. Partridge, A.P. Pathak, A.C. Peet, S. Punwani, A.R. Reynolds, S.P. Robinson, L.K. Shankar, R.A. Sharma, D. Soloviev, S. Stroobants, D.C. Sullivan, S.A. Taylor, P.S. Tofts, G.M. Tozer, M. Van Herk, S. Walker-samuel, J. Wason, K.J. Williams, P. Workman, T.E. Yankeelov, K.M. Brindle, L.M. Mcshane, A. Jackson, J.C. Waterton, Imaging biomarker roadmap for cancer studies, Nat. Publ. Gr. 14 (2016) 169–186, https://doi.org/10.1038/nrclinonc.2016.162.

[16] S. Zwick, G. Brix, P.S. Tofts, R. Strecker, A. Kopp-Schneider, H. Laue, W. Semmler, F. Kiessling, Simulation-based comparison of two approaches frequently used for dynamic contrast-enhanced MRI, Eur. Radiol. 20 (2010) 432–442, https://doi.org/10.1007/s00330-009-1556-6.

[17] E. Ashton, T. McShane, J. Evelhoch, Inter-operator variability in perfusion assessment of tumors in MRI using automated AIF detection, Lect. Notes Comput. Sci. (Including Subser. Lect. Notes Artif. Intell. Lect. Notes Bioinformatics). 3749 LNCS, (2005), pp. 451–458, https://doi.org/10.1007/11566465_56.

[18] M. Ingrisch, O. Dietrich, U.I. Attenberger, K. Nikolaou, S. Sourbron, M.F. Reiser, C. Fink, Quantitative pulmonary perfusion magnetic resonance imaging: influence of temporal resolution and signal-to-noise ratio, Invest. Radiol. 45 (2010) 7–14, https://doi.org/10.1097/RLI.0b013e3181bc2d0c.

[19] M.C. Schabel, G.R. Morrell, Uncertainty in T1 mapping using the variable flip angle method with two flip angles, Phys. Med. Biol. 54 (2009), https://doi.org/10.1088/0031-9155/54/1/N01.

[20] I.A. Mendichovszky, M. Cutajar, I. Gordon, Reproducibility of the aortic input function (AIF) derived from dynamic contrast-enhanced magnetic resonance imaging (DCE-MRI) of the kidneys in a volunteer study, Eur. J. Radiol. 71 (2009) 576–581, https://doi.org/10.1016/j.ejrad.2008.09.025.

[21] K. Cheng, P.J.B. Koeck, H. Elmlund, K. Idakieva, K. Parvanova, H. Schwarz, T. Ternström, H. Hebert, Rapid high-resolution T1 mapping by variable flip angles: accurate and precise measurements in the presence of radiofrequency field inhomogeneity, Magn. Reson. Med. 55 (2006) 566–576, https://doi.org/10.1002/mrm.20791.

[22] P. Di Giovanni, C.A. Azlan, T.S. Ahearn, S.I. Semple, F.J. Gilbert, T.W. Redpath, The accuracy of pharmacokinetic parameter measurement in DCE-MRI of the breast at 3 T, Phys. Med. Biol. 55 (2010) 121–132, https://doi.org/10.1088/0031-9155/55/1/008.

[23] M. Quentin, C. Arsov, S. Rohlen, J. Klasen, G. Antoch, P. Albers, D. Blondin, Inter-reader agreement of multi-parametric MR imaging for the detection of prostate cancer: evaluation of a scoring system, Fortschr. Röntgenstr. 184 (2012) 925–929, https://doi.org/10.1055/s-0032-1312876.

[24] S.H. Polanec, T.H. Helbich, M. Margreiter, H.C. Klingler, K. Kubin, M. Susani, K. Pinker-Domenig, P. Brader, Magnetic resonance imaging-guided prostate biopsy: institutional analysis and systematic review, Rofo 186 (2014) 501–507, https://doi.org/10.1055/s-0033-1355546.

[25] J. Epstein, J.W. Allsbrook, M. Amin, D.L. Egeva, ISUP Grading Committee, The 2005 international society of urological pathology (ISUP) consensus conference on glea- son grading of prostatic carcinoma, Eur. Urol. 49 (2006) 754–759, https://doi.org/10.1200/JCO.2005.05.525.

[26] M.S. Davenport, T. Heye, B.M. Dale, J.J. Horvath, S.R. Breault, S. Feuerlein, M.R. Bashir, D.T. Boll, E.M. Merkle, Inter- and intra-rater reproducibility of quantitative dynamic contrast enhanced MRI using TWIST perfusion data in a uterine fibroid model, J. Magn. Reson. Imaging 38 (2013) 329–335, https://doi.org/10.1002/jmri.23974.

[27] H.C. Rischke, U. Nestle, T. Fechter, C. Doll, N. Volegova-Neher, K. Henne, J. Scholber, S. Knippen, S. Kirste, A.L. Grosu, C.A. Jilg, 3 Tesla multiparametric MRI for GTV-definition of dominant intraprostatic lesions in patients with prostate cancer—an interobserver variability study, Radiat. Oncol. 8 (2013) 1, https://doi.org/10.1186/1748-717X-8-183.

[28] P. Andrzejewski, P. Kuess, B. Knäusl, K. Pinker, P. Georg, J. Knoth, D. Berger, C. Kirisits, G. Goldner, T. Helbich, R. Pötter, D. Georg, Feasibility of dominant intraprostatic lesion boosting using advanced photon-, proton- or brachytherapy, Radiother. Oncol. 117 (2015) 509–514, https://doi.org/10.1016/j.radonc.2015.07.028.

[29] E.N.J.T. van Lin, J.J. Fütterer, S.W.T.P.J. Heijmink, L.P. van der Vight, A.L. Hoffmann, P. van Kollenburg, H.J. Huisman, T.W.J. Scheenen, J.A. Witjes, J.W. Leer, J.O. Barentsz, A.G. Visser, IMRT boost dose planning on dominant intraprostatic lesions: gold marker-based three-dimensional fusion of CT with dynamic contrast-enhanced and 1H-spectroscopic MRI, Int. J. Radiat. Oncol. Biol. Phys. 65 (2006) 291–303, https://doi.org/10.1016/j.ijrobp.2005.12.046.

[30] S. Woo, C.H. Suh, S.Y. Kim, J.Y. Cho, S.H. Kim, M.H. Moon, Head-to-head comparison between biparametric and multiparametric MRI for the diagnosis of prostate cancer: a systematic review and meta-analysis, Am. J. Roentgenol. 211 (2018) W226–W241, https://doi.org/10.2214/AJR.18.19880.